

# UC Santa Barbara

## UC Santa Barbara Previously Published Works

### Title

Quantum Hall effect of the topological insulator state of cadmium arsenide in Corbino geometry

### Permalink

<https://escholarship.org/uc/item/1tc875jm>

### Journal

Applied Physics Letters, 118(26)

### ISSN

0003-6951 1077-3118

### Authors

Galletti, Luca  
Rashidi, Arman  
Kealhofer, David A  
[et al.](#)

### Publication Date

2021-06-28

### DOI








10.1063/5.0056357

Peer reviewed

# Quantum Hall effect of the topological insulator state of cadmium arsenide in Corbino geometry

Cite as: Appl. Phys. Lett. **118**, 261901 (2021); <https://doi.org/10.1063/5.0056357>

Submitted: 09 May 2021 . Accepted: 04 June 2021 . Published Online: 28 June 2021

 Luca Galletti,  Arman Rashidi,  David A. Kealhofer, Manik Goyal,  Binghao Guo,  Yuntian Li, Chen Shang,  John E. Bowers, and  Susanne Stemmer

## COLLECTIONS

 This paper was selected as an Editor's Pick



View Online



Export Citation



CrossMark



Webinar  
How to Characterize Magnetic Materials Using Lock-in Amplifiers

 Zurich Instruments



[Register now](#)

# Quantum Hall effect of the topological insulator state of cadmium arsenide in Corbino geometry

Cite as: Appl. Phys. Lett. **118**, 261901 (2021); doi: [10.1063/5.0056357](https://doi.org/10.1063/5.0056357)

Submitted: 9 May 2021 · Accepted: 4 June 2021 ·

Published Online: 28 June 2021



View Online



Export Citation



CrossMark

Luca Galletti,<sup>1</sup>  Arman Rashidi,<sup>1</sup>  David A. Kealhofer,<sup>1</sup>  Manik Goyal,<sup>1</sup>  Binghao Guo,<sup>1</sup>  Yuntian Li,<sup>1</sup>   
Chen Shang,<sup>2</sup>  John E. Bowers,<sup>2</sup>  and Susanne Stemmer<sup>1,a)</sup> 

## AFFILIATIONS

<sup>1</sup>Materials Department, University of California, Santa Barbara, California 93106-5050, USA

<sup>2</sup>Department of Electrical and Computer Engineering, University of California, Santa Barbara, Santa Barbara, California 93106-9560, USA

<sup>a)</sup>Author to whom correspondence should be addressed: [stemmer@mrl.ucsb.edu](mailto:stemmer@mrl.ucsb.edu)

## ABSTRACT

The surfaces of a three-dimensional topological insulator each host a single Dirac fermion, which, in a strong magnetic field, contribute to the transverse conductance in integer-and-a-half multiples of the conductance quantum. The direct observation of this extra half integer, the hallmark of the two-dimensional Dirac state, is usually thwarted by the fermion doubling theorem—top and bottom surfaces are not measured independently. Here, we employ a Corbino measurement geometry in which a current, induced by an ac magnetic field, is driven around the ring, as a complementary measurement to the conventional Hall bar geometry. As the device enters the quantum Hall regime, the transverse voltage reaches a series of plateaus when the current is carried by the incompressible bulk states. We compare the results with the corresponding Hall bar measurements.

Published under an exclusive license by AIP Publishing. <https://doi.org/10.1063/5.0056357>

In a strong enough magnetic field, the massless fermions on the surfaces of a three-dimensional topological insulator (TI)<sup>1,2</sup> each contribute to the transverse conductance in integer-and-a-half multiples of the conductance quantum.<sup>3,4</sup> The direct observation of this extra half integer, a fingerprint of the two-dimensional Dirac state, is thwarted by the fermion doubling theorem; absent strong electron–electron correlations, only integer filling factors can be observed in the quantum Hall effect,<sup>5–7</sup> just like in a conventional two-dimensional electron system. An integer quantum Hall effect has been observed in several different topological insulators in standard Hall bar geometries.<sup>8–12</sup> Since the surface of a three-dimensional topological insulator is the interface between two regions whose band structures have different topological invariants, electrical contacts and device isolation do not add edges.<sup>13</sup> For this reason, the nature and location of the edge states of a topological insulator, which carry the current in the conventional picture of the quantum Hall effect,<sup>14,15</sup> has been a subject of substantial discussion in the literature.<sup>13,16–22</sup>

An alternative measurement geometry is a Corbino ring, consisting of two concentric metal contacts on top of a much larger mesa, as shown in Fig. 1(a). When current is driven from the center electrode to the outer ring, magnetoresistance measurements probe the diagonal element of the conductance tensor ( $G_{xx}$ ), according to  $V_r = I_r/G_{xx}$ ,

where  $V_r$  is the voltage across the ring and  $I_r$  is the current. The Hall effect is not measured. By inductively coupling a small ac magnetic field out of plane to the disk, however, an *azimuthal* current induces a voltage ( $V_r$ ) between the inner and outer contacts that is related to the Hall voltage.<sup>23</sup> With the current, thus, azimuthally biased, the Corbino ring is in effect a local probe of the topological surface, although the bottom and top surfaces may still couple capacitively. Moreover, because charge is transported across the ring through the two-dimensional bulk of the quantum Hall insulator, it is edgeless: no charge is transported through states at the edges of the contacts.

Our experiments are carried out on thin films of cadmium arsenide ( $\text{Cd}_3\text{As}_2$ ), which is called a three-dimensional Dirac semimetal because, in its bulk electronic structure, two doubly degenerate bands cross.<sup>24–27</sup> In this work, the salient feature is the band inversion. In thin films, the bulk electronic structure demonstrates a gap, and the band structure is characterized by a  $\mathbb{Z}_2$  invariant of nontrivial value.<sup>24</sup> The (001) surfaces of these films, as a result, feature topological insulator-like surface states [see Fig. 1(a)].<sup>12,24</sup> Quantum Hall measurements performed on gated Hall bar structures reveal filling factor sequences corresponding to two sets of Landau levels, each from a single Dirac state, originating from the top and bottom surfaces, respectively.<sup>12</sup> Here, we compare results obtained from the same film in quasi-

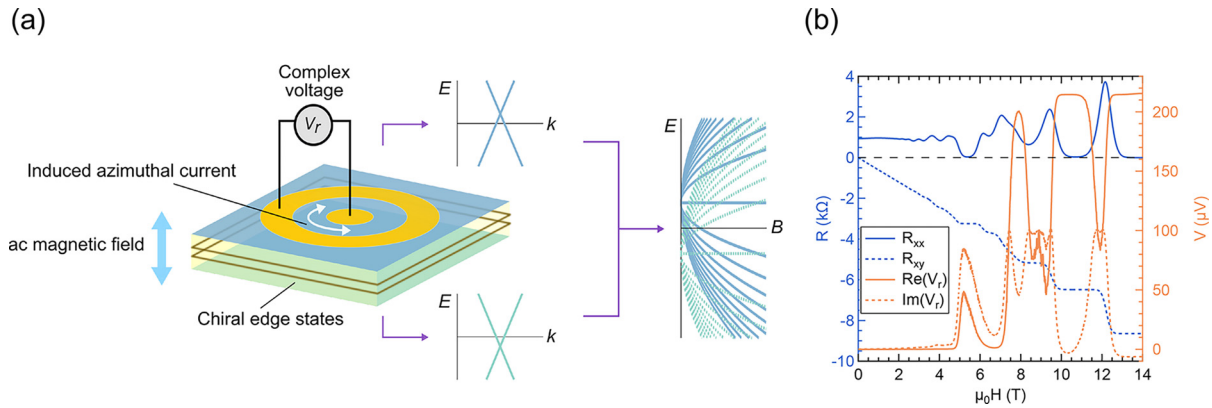


**FIG. 1.** Inductively coupled ac Corbino disk measurements on a topological insulator surface. (a) Schematic of the top and bottom surface Dirac nodes of a TI, which are offset in energy due to the asymmetry of the heterostructure, and the resulting two sets of Landau levels when the TI is placed in a magnetic field. Also shown is a schematic of the inductively coupled measurement on a topological insulator placed in a magnetic field. An oscillating magnetic field induces an azimuthal electric field, which creates azimuthal currents circulating around the ring-shaped channel. An induced transverse voltage  $V_r$  is measured with a lock-in amplifier. (b) Measured real and imaginary components of  $V_r$  as a function of the external field  $H$ . Longitudinal and transverse resistivity measured on a Hall bar device are shown on the same plot. The filling factors corresponding to the quantum Hall plateaus of the Hall bar are indicated.

dc magnetoresistance measurements on Hall bars and Corbino disks and the inductive ac technique described above [Fig. 1(b)].

The (001) thin films of  $\text{Cd}_3\text{As}_2$  were grown by molecular beam epitaxy (MBE) on (001) GaSb substrates. Details of the MBE growth have been described elsewhere.<sup>28,29</sup> A 500 nm  $\text{Al}_{0.45}\text{In}_{0.55}\text{Sb}$  layer was used as a buffer layer between the  $\text{Cd}_3\text{As}_2$  and the substrate to provide electrical insulation and reduce extended defect densities in the  $\text{Cd}_3\text{As}_2$  layer. The composition of the buffer layer was chosen because the lattice parameter of  $\text{Al}_{0.45}\text{In}_{0.55}\text{Sb}$  matches the in-plane lattice parameter of  $\text{Cd}_3\text{As}_2$ . Results presented focus on measurements performed on a 30 nm-thick film, which was capped *in situ* with 3 nm of GaSb. In total, eight films with thicknesses between 20 and 70 nm were measured, including samples with different buffer layers. In general, films thinner than 40 nm showed well-developed quantum Hall plateaus and  $R_{xx}$  was sufficiently low for magnetic coupling measurements.

Hall bars with dimensions of  $100 \times 300 \mu\text{m}$  and Corbino disks of different external and internal radii (300/200, 300/250, and 200/150  $\mu\text{m}$ ) were fabricated using photolithographic techniques. Ohmic Ti/Au (500/2500 Å) contacts were patterned by lift off. Mesa isolation was accomplished by  $\text{Ar}^+$  ion milling. After device fabrication, the sample was annealed in vacuum at 120 °C and a 30 nm  $\text{AlO}_x$  film was deposited for passivation using atomic layer deposition. The Hall carrier density for the film discussed in the main body was  $1 \times 10^{12} \text{cm}^{-2}$ , and the Hall mobility was  $2 \text{m}^2/\text{Vs}$  at 2 K.

Quasi-dc magnetoresistance measurements were performed at 40 mK in a dilution refrigerator on a Hall bar and four Corbino disks of different sizes, all fabricated at the same time on the 30 nm  $\text{Cd}_3\text{As}_2$  film, using standard lock-in techniques. Data shown here were acquired from the Corbino disk with internal radius  $r_2 = 250$  and external radius  $r_1 = 300 \mu\text{m}$ . An external magnetic field  $\mu_0\mathbf{H}$  of up to 14 T was applied out of plane. Measurements at higher temperatures ( $T > 1$  K) were performed with a Quantum Design PPMS Dynacool system with a 14 T magnet.

Magnetic coupling measurements were performed using a small ac magnetic field to induce azimuthal currents by mutual inductance.  $\Re(V_r)$  and  $\Im(V_r)$  were measured between the inner and the outer

electrodes. The ac field was generated by a small NbTi coil, made by winding a NbTi multifilament wire [0.50 diameter, 20 mm insulation layer ( $3.0 \pm 0.1/1$  Co/NbTi ratio)] into a solenoid of 80 turns with a 5 bore and a 16 mm external diameter. The solenoid was placed directly under the sample, with the Corbino disk aligned to the bore axis. Magnetic coupling measurements shown here were performed on a Corbino disk with radii  $r_2 = 150$  and  $r_1 = 200 \mu\text{m}$ .  $R_{xx}$  and magnetic coupling voltages were nearly symmetric upon magnetic field inversion, while  $R_{xy}$  was antisymmetric, with deviations on the order of 10% for  $R_{xx}$  and less than 1% in all other cases. Symmetrization or anti-symmetrization of the data was performed after interpolation.

Figure 2 shows data from the quasi-dc measurements. In the Hall bar measurement [Fig. 2(a)], quantum Hall plateaus with filling factors  $\nu_H = 3, 4, 5, 7,$  and  $8$  appear at fields above 2 T. From the longitudinal and transverse magnetoresistances ( $R_{xx}$  and  $R_{xy}$ ), the diagonal term of the conductivity tensor ( $G_{xx}$ ) can be obtained to compare to that measured in the Corbino disk,

$$G_{xx} = \frac{\log(r_1/r_2)}{2\pi R_r}, \quad (1)$$

where  $R_r$  is the two-terminal resistance of the disk and  $r_1 > r_2$  are its external and internal radii, respectively. Figure 2(b) demonstrates good agreement of  $G_{xx}$  in both geometries, allowing us to assign filling factors in the dc Corbino disk data using the plateaus measured in the Hall bar.

As shown in Ref. 12, the filling factor sequences can be understood in terms of two intersecting Landau fans that originate from the Dirac states on the top and bottom surfaces, respectively. Only odd-integer plateaus are expected for perfectly degenerate surfaces;<sup>13</sup> in general, however, the top and bottom surfaces/interfaces in a heterostructure differ by an energy difference, and all filling factors will be present except for accidental degeneracies.<sup>8,9,12</sup>

A simple model is shown in Figs. 3(a) and 3(b). Each surface hosts a single Dirac fermion, so that  $\nu_B$  (or  $\nu_T$ ) =  $(n + 1/2)$ , where  $n$  is the Landau level index.<sup>3,4</sup> The filling factor sequence in the Hall bar,  $\nu_H = 3, 4,$  and  $5$ , can be assigned to  $\nu_B = 5/2, 7/2,$  and  $9/2$ , while

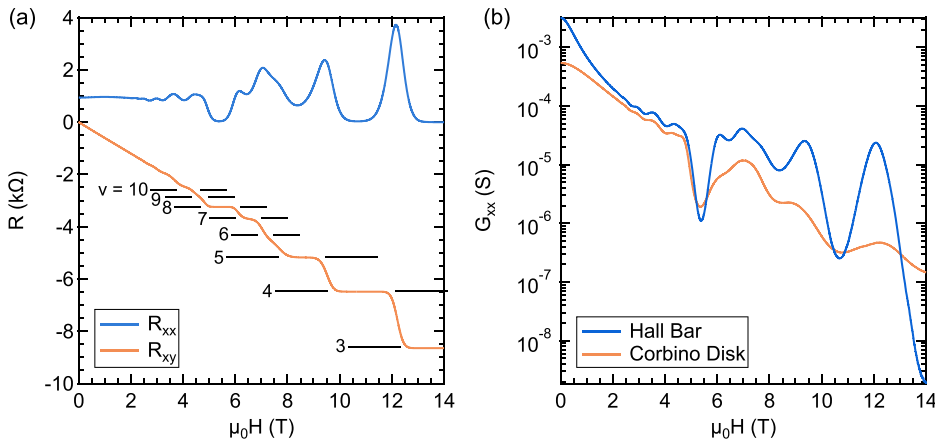


**FIG. 2.** Hall bar and Corbino disk dc measurements. (a)  $R_{xx}$  and  $R_{xy}$  measured in Hall bar geometry. Horizontal lines indicate the quantum Hall plateaus. (b) Diagonal element of the conductivity tensor,  $G_{xx}$ , extracted from the measurements of the Hall bar and the Corbino disks, respectively.

$\nu_T = 1/2$  for all three values of  $\nu_H$ . The model and Landau level gaps extracted from it [Fig. 3(c)] naturally explain the suppression of  $\nu_H = 6$  with the crossing of Landau levels from different surfaces, which reduces the Landau level gap, as well as the relative prominence of other transitions (e.g.,  $\nu_H = 8$  is more prominent than  $\nu_H = 7$  and

$\nu_H = 3$  more prominent than  $\nu_H = 4$ ). The gaps can be compared qualitatively with the activation energies from the two measurements, deduced from a fit of the temperature dependence of the  $G_{xx}$  minima [Figs. 3(d) and 3(e)]. Even though the extracted values [Fig. 3(f)] do not correspond to the actual Landau level gaps (e.g., disorder reduces

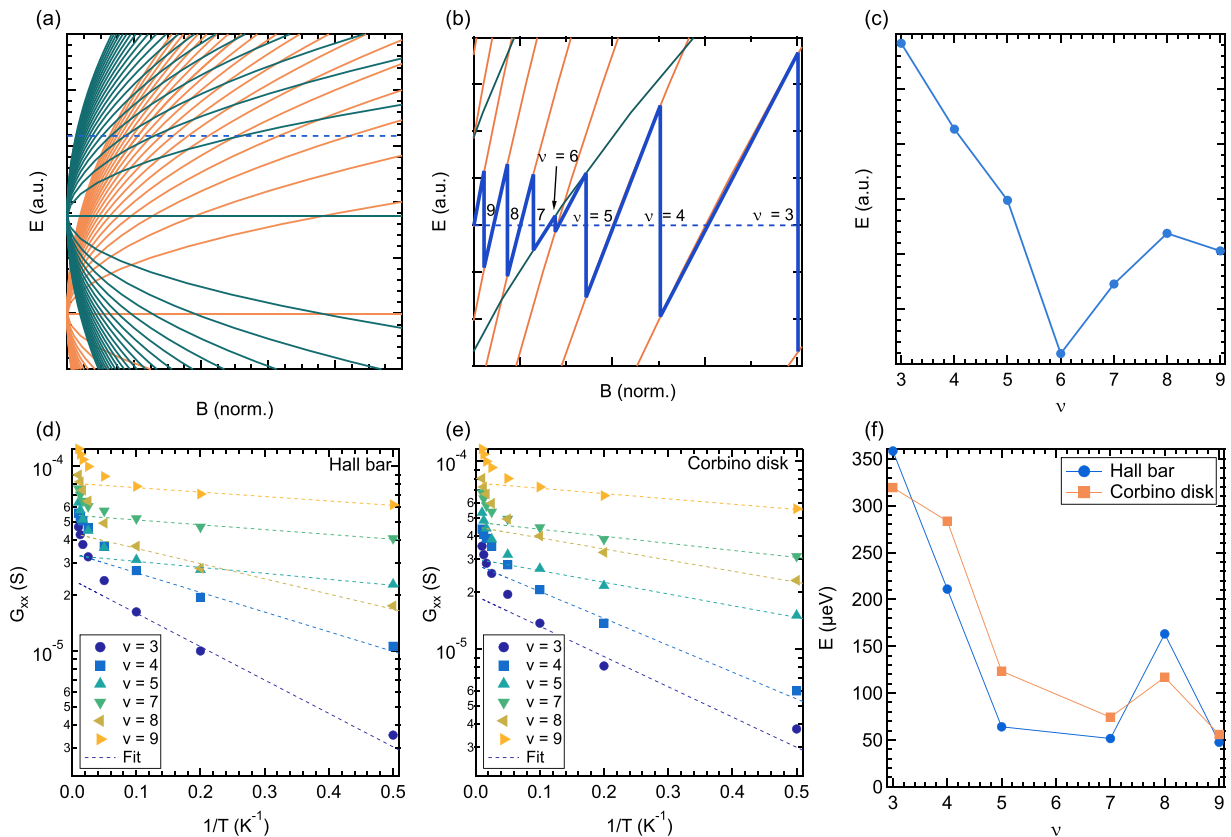


**FIG. 3.** Landau level fan diagram consistent the filling factors observed in the Hall bar measurements of the topological insulator-like state of a thin film of  $Cd_3As_2$ . (a) Schematic model of Landau levels from the topological surface states from top and bottom surfaces for the case where the two surfaces are at a slightly different potential due to the inherent asymmetry of the heterostructure.<sup>12</sup> (b) Magnified section of A showing the resulting sequence of filling factors in a magnetic field sweep. (c) Landau energy gaps extracted from the model for each filling factor show a remarkable agreement with experimental data in (f). (d) and (e) Arrhenius plots of  $G_{xx}$  for the Hall bar and Corbino disk, respectively. (f) Activation energies for  $G_{xx}$  minima at different filling factors.

them<sup>30</sup>), the dependence of the relative values on the filling factor supports the underlying model of the surface states detailed in Figs. 3(a) and 3(b).

The general agreement between the two measurement geometries shows that the Landau level sequences reflect contributions from the massless states on both surfaces also for the Corbino disk. The agreement is a direct consequence of the three-dimensional nature of the topological insulator surfaces<sup>13</sup> and the resistive coupling of all surfaces in both measurement geometries.

We next turn to the inductively coupled measurements. Real and imaginary components of the Hall voltage  $V_r$  were measured between the inner and outer edges of the disk. Here,  $V_r$  is given by<sup>23</sup>

$$V_r = \frac{\omega MR_{xy}}{(R_{xx} + j\omega L)(1 - j\omega CZ)}, \quad (2)$$

where  $M$  is the mutual inductance between the coil and the Corbino disk,  $I_m$  is the coil ac current,  $\frac{\omega}{2\pi}$  is the frequency of the ac field,  $C$  is the total series capacitance of the system, and  $L$  is the self-inductance of the disk. The capacitance  $C$  includes the capacitance between the metal rings and the capacitance of the probing wires. The capacitance between the metal rings of the Corbino disk is negligible in our

microscopic Corbino disks, so that  $C$  mainly reflects the capacitance of the probing wires. The complex impedance,  $Z$ , takes the form:<sup>23</sup>

$$Z = \frac{R_{xx}^2 + R_{xy}^2 + j\omega LR_{xx}}{R_{xx} + j\omega L}, \quad (3)$$

with  $j^2 = -1$ . In the quantum Hall regime ( $R_{xx} \approx 0$ ), the Corbino ring behaves as a pure inductance and  $V_r$  is proportional to the azimuthal current via the Hall resistance.<sup>23</sup> The appearance of the Hall plateaus in the magnetic coupling experiments is illuminated by Eq. (2). The value of  $\Re(V_r)$  in the plateaus is closely related to the off diagonal element of the conductance tensor  $G_{ij}$ . In the limit where  $R_{xx} \ll \omega L$  and  $\omega CZ \gg 1$ , Eq. (2) simplifies to  $V_r = -\frac{MI_m}{CR_{xy}}$  and  $\Re(V_r)$  scales with the conductance quantum  $ve^2/h$ , where  $e$  is the electron charge and  $h$  is Planck's constant.

The left column of Fig. 4 shows the results at different frequencies. At high frequencies ( $\omega \gg R_{xx}/L$ ),  $\Re(V_r)$  shows well-developed plateaus that coincide with the quantum Hall plateaus,  $\nu_H = 4$  and  $\nu_H = 3$  [see Fig. 1(b) for a direct comparison]. Smaller peaks, rather than saturating plateaus, form at higher filling factors due to a non-

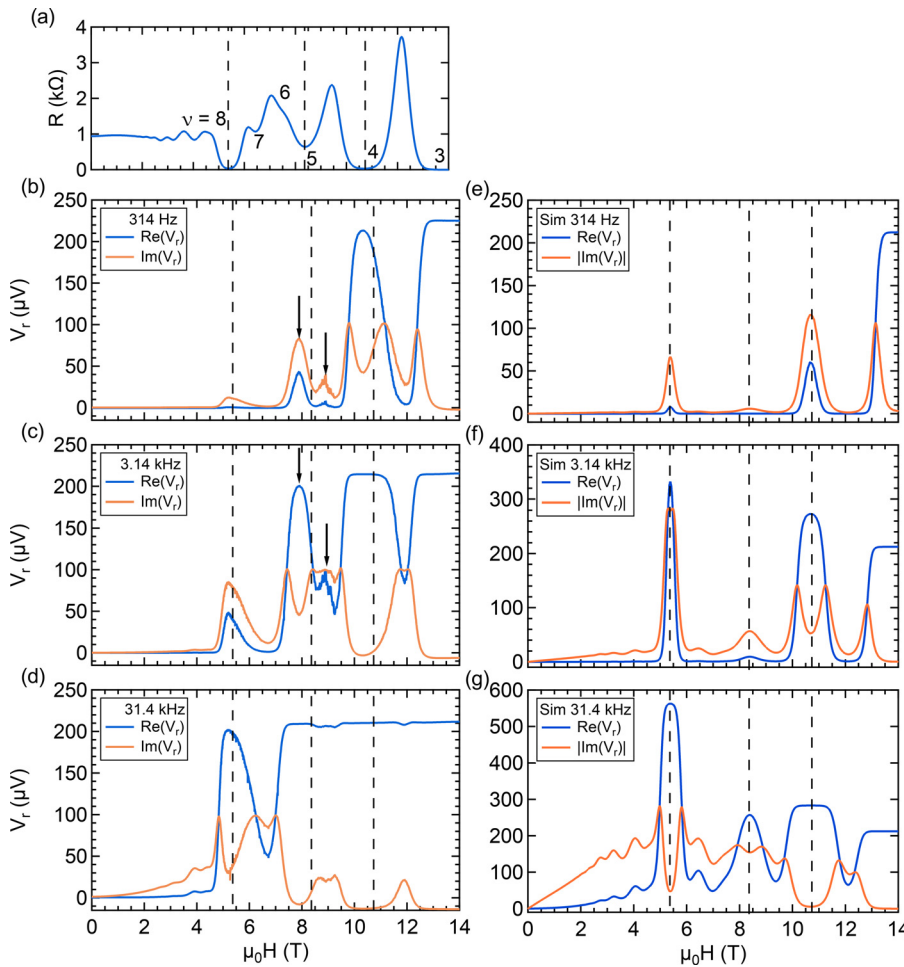


**FIG. 4.** Corbino disk magnetic coupling measurements and calculations. (a) Hall bar resistivity measurement shown as reference [same data as shown in Fig. 3(a)]. (b)–(d) Magnetic coupling measurements at 0.314, 3.14, and 31.4 kHz, respectively. Dashed lines indicate the positions of the minima in a for  $\nu_H = 4, 5$ , and  $8$ , which correspond to the center of the Hall plateaus in the Hall bar measurements shown in Fig. 2(a). Black arrows indicate features around  $\nu_H = 5$  and  $\nu_H = 6$ , where the data differs from the Hall bar measurements (see the text). (e)–(g) Calculations using the experimental frequencies and Hall bar data as input. In these calculations,  $L = 5$ ,  $M = 350$  nH, and  $C = 200$  pF. Dashed lines indicate the positions of the minima in (a) for  $\nu_H = 4, 5$ , and  $8$ , drawn at the center of the Hall plateaus in the Hall bar measurements shown in Fig. 2(a).

zero  $R_{xx}$ , meaning that the device is not in the high-frequency condition ( $\omega \gg R_{xx}/L$ ). Increasing the frequency should increase the amplitude, as is indeed observed [see Figs. 4(c) and 4(d)]. Peaks in  $\Im m(V_r)$  flank the plateaus.

Figure 4 (right column) compares the experimental data with calculations using Eqs. (2) and (3) and the experimental  $R_{xx}$  and  $R_{xy}$  data from the Hall bar measurements as input. The calculations capture many features of the experiments. For example, they reproduce the peaks and plateaus in  $\Re e(V_r)$  and their frequency behavior, including the widening of plateaus at higher frequencies. The corresponding peaks in  $\Im m(V_r)$  are reproduced as well.

The calculations differ in crucial aspects from the experimental observations. In particular,  $\nu_H = 5$  is a prominent plateau in the Hall bar measurements and, therefore, in the calculations, which use the Hall data as input. In the ac measurement, there is only a small peak, while a more pronounced one appears at a position closer to  $\nu_H = 6$ , which is nearly absent in the Hall bar measurements. At  $\nu_H = 8$ , when the top surface has increased its filling factor by one, calculations and experiments match again. Moreover, in the experimental data, the amplitudes of the plateaus saturate to the same constant value ( $\sim 215 \mu\text{V}$ ), in contrast to the calculations. The constant amplitude of the plateaus could not be reproduced by artificially tuning the device-dependent quantities  $C$ ,  $L$ , and  $M$  in the calculations. A constant amplitude of the Hall plateaus was observed in several other samples, and the reasons are not well understood at present. Prior experiments on conventional two-dimensional electron gases also noted that the plateaus did not scale with the conductance quantum as would be expected from Eq. (2).<sup>23</sup> This precludes an independent determination of the filling factor from the measured value of  $V_r$ .

Despite this issue, the results show that the behavior of the Hall voltage in the ac Corbino measurement reflects the transitions of the bulk of the two-dimensional electron system as the field is swept, with the plateaus corresponding to the incompressible state of the bulk of the quantum Hall insulator. The main finding is, therefore, that the Hall bar and ac Corbino measurements largely agree with each other, despite the fact that transport is edgeless in the latter. This confirms a picture of the quantum Hall effect of a topological insulator featuring an incompressible bulk and well-defined edge states, despite the fact that the side surfaces may not gap out in the perpendicular field. This picture is in agreement with that of most theoretical studies for topological insulators that are not too thick. Future studies should investigate the origins of the discrepancies between the two measurements near  $\nu_H = 6$  and the quantification of the induced voltage in the ac Corbino measurement in terms of the filling factor of the surface(s).

The research was primarily supported by a Vannevar Bush Faculty Fellowship program of the U.S. Department of Defense (Grant No. N00014-16-1-2814) and by the U.S. Army Research Office (Grant No. W911NF-16-1-0280). B. Guo thanks the UCSB Quantum Foundry for support, which is funded via the Q-AMASE-i program of the U.S. National Science Foundation under Award No. DMR-1906325. The research made use of shared facilities of the UCSB MRSEC (No. NSF DMR 1720256).

#### DATA AVAILABILITY

The data that support the findings of this study are available within the article.

#### REFERENCES

1. L. Fu, C. L. Kane, and E. J. Mele, "Topological insulators in three dimensions," *Phys. Rev. Lett.* **98**, 106803 (2007).
2. J. E. Moore and L. Balents, "Topological invariants of time-reversal-invariant band structures," *Phys. Rev. B* **75**, 121306 (2007).
3. R. Jackiw, "Fractional charge and zero modes for planar systems in a magnetic field," *Phys. Rev. D* **29**, 2375–2377 (1984).
4. A. M. J. Schakel, "Relativistic quantum Hall effect," *Phys. Rev. D* **43**, 1428–1431 (1991).
5. H. B. Nielsen and M. Ninomiya, "The Adler-Bell-Jackiw anomaly and Weyl fermions in a crystal," *Phys. Lett. B* **130**, 389–396 (1983).
6. D. J. Thouless, M. Kohmoto, M. P. Nightingale, and M. Denny, "Quantized Hall conductance in a two-dimensional periodic potential," *Phys. Rev. Lett.* **49**, 405–408 (1982).
7. F. D. M. Haldane, "Model for a quantum Hall effect without Landau Levels: Condensed-matter realization of the 'parity anomaly,'" *Phys. Rev. Lett.* **61**, 2015–2018 (1988).
8. C. Brüne, C. X. Liu, E. G. Novik, E. M. Hankiewicz, H. Buhmann, Y. L. Chen, X. L. Qi, Z. X. Shen, S. C. Zhang, and L. W. Molenkamp, "Quantum Hall effect from the topological surface states of strained bulk HgTe," *Phys. Rev. Lett.* **106**, 126803 (2011).
9. Y. Xu, I. Miotkowski, C. Liu, J. F. Tian, H. Nam, N. Alidoust, J. N. Hu, C. K. Shih, M. Z. Hasan, and Y. P. Chen, "Observation of topological surface state quantum Hall effect in an intrinsic three-dimensional topological insulator," *Nat. Phys.* **10**, 956–963 (2014).
10. R. Yoshimi, A. Tsukazaki, Y. Kozuka, J. Falson, K. S. Takahashi, J. G. Checkelsky, N. Nagaosa, M. Kawasaki, and Y. Tokura, "Quantum Hall effect top bottom surface states topological insulator (Bi<sub>1-x</sub>Sb<sub>x</sub>)<sub>2</sub>Te<sub>3</sub> films," *Nat. Commun.* **6**, 6627 (2015).
11. N. Koirala, M. Brahlek, M. Salehi, L. Wu, J. X. Dai, J. Waugh, T. Nummy, M. G. Han, J. Moon, Y. M. Zhu, D. Dessau, W. D. Wu, N. P. Armitage, and S. Oh, "Record surface state mobility and quantum Hall effect in topological insulator thin films via interface engineering," *Nano Lett.* **15**, 8245–8249 (2015).
12. D. A. Kealhofer, L. Galletti, T. Schumann, A. Suslov, and S. Stemmer, "Topological insulator state and collapse of the quantum Hall effect in a three-dimensional Dirac semimetal heterojunction," *Phys. Rev. X* **10**, 011050 (2020).
13. D. H. Lee, "Surface states of topological insulators: The Dirac fermion in curved two-dimensional spaces," *Phys. Rev. Lett.* **103**, 196804 (2009).
14. M. Büttiker, "Absence of backscattering in the quantum Hall effect in multiprobe conductors," *Phys. Rev. B* **38**, 9375–9389 (1988).
15. B. I. Halperin, "Quantized Hall conductance, current-carrying edge states, and the existence of extended states in a two-dimensional disordered potential," *Phys. Rev. B* **25**, 2185–2190 (1982).
16. O. Vafek, "Quantum Hall effect in a singly and doubly connected three-dimensional topological insulator," *Phys. Rev. B* **84**, 245417 (2011).
17. R. L. Chu, J. R. Shi, and S. Q. Shen, "Surface edge state and half-quantized Hall conductance in topological insulators," *Phys. Rev. B* **84**, 085312 (2011).
18. M. Sitte, A. Rosch, E. Altman, and L. Fritz, "Topological insulators in magnetic fields: Quantum Hall effect and edge channels with a nonquantized theta term," *Phys. Rev. Lett.* **108**, 126807 (2012).
19. Y. Y. Zhang, X. R. Wang, and X. C. Xie, "Three-dimensional topological insulator in a magnetic field: Chiral side surface states and quantized Hall conductance," *J. Phys.: Condens. Matter* **24**, 015004 (2012).
20. E. J. König, P. M. Ostrovsky, I. V. Protodopov, I. V. Gornyi, I. S. Burmistrov, and A. D. Mirlin, "Half-integer quantum Hall effect of disordered Dirac fermions at a topological insulator surface," *Phys. Rev. B* **90**, 165435 (2014).
21. T. Morimoto, A. Furusaki, and N. Nagaosa, "Charge and spin transport in edge channels of a  $\nu = 0$  quantum Hall system on the surface of topological insulators," *Phys. Rev. Lett.* **114**, 146803 (2015).
22. K. Hattori and H. Okamoto, "Chiral surface modes in three-dimensional topological insulators," *J. Phys. Soc. Jpn.* **85**, 053707 (2016).
23. B. Jeanneret, B. D. Hall, H. J. Buhlmann, R. Houdre, M. Ilegems, B. Jeckelmann, and U. Feller, "Observation of the integer quantum Hall-effect by magnetic coupling to a Corbino ring," *Phys. Rev. B* **51**, 9752–9756 (1995).
24. Z. J. Wang, H. M. Weng, Q. S. Wu, X. Dai, and Z. Fang, "Three-dimensional Dirac semimetal and quantum transport in Cd<sub>3</sub>As<sub>2</sub>," *Phys. Rev. B* **88**, 125427 (2013).

- <sup>25</sup>M. N. Ali, Q. Gibson, S. Jeon, B. B. Zhou, A. Yazdani, and R. J. Cava, "The crystal and electronic structures of  $\text{Cd}_3\text{As}_2$ , the three-dimensional electronic analogue of graphene," *Inorg. Chem.* **53**, 4062 (2014).
- <sup>26</sup>M. Neupane, S. Y. Xu, R. Sankar, N. Alidoust, G. Bian, C. Liu, I. Belopolski, T. R. Chang, H. T. Jeng, H. Lin, A. Bansil, F. Chou, and M. Z. Hasan, "Observation of a three-dimensional topological Dirac semimetal phase in high-mobility  $\text{Cd}_3\text{As}_2$ ," *Nat. Commun.* **5**, 3786 (2014).
- <sup>27</sup>Z. K. Liu, J. Jiang, B. Zhou, Z. J. Wang, Y. Zhang, H. M. Weng, D. Prabhakaran, S.-K. Mo, H. Peng, P. Dudin, T. Kim, M. Hoesch, Z. Fang, X. Dai, Z. X. Shen, D. L. Feng, Z. Hussain, and Y. L. Chen, "A stable three-dimensional topological Dirac semimetal  $\text{Cd}_3\text{As}_2$ ," *Nat. Mater.* **13**, 677–681 (2014).
- <sup>28</sup>T. Schumann, M. Goyal, H. Kim, and S. Stemmer, "Molecular beam epitaxy of  $\text{Cd}_3\text{As}_2$  on a III-V substrate," *APL Mater.* **4**, 126110 (2016).
- <sup>29</sup>D. A. Kealhofer, H. Kim, T. Schumann, M. Goyal, L. Galletti, and S. Stemmer, "Basal-plane growth of cadmium arsenide by molecular beam epitaxy," *Phys. Rev. Mater.* **3**, 031201 (2019).
- <sup>30</sup>T. Ando, A. B. Fowler, and F. Stern, "Electronic properties of two-dimensional systems," *Rev. Mod. Phys.* **54**, 437–672 (1982).